Supervised learning of soliton X-junctions in lithium niobate films on insulator

Alessandro Bile,[1] **Mathieu Chauvet,**[2] **Hamed Tari,**[1] [ID] **and Eugenio Fazio**[1,*] [ID]

[1]*Department of Fundamental and Applied Sciences for Engineering, Sapienza University of Rome, Via A. Scarpa 16, Rome, Italy*
[2]*FEMTO-ST Institute, UMR CNRS 6174, University of Franche-Comté, 15B Avenue des Montboucons, 25000 Besançon, France*
*Corresponding author: eugenio.fazio@uniroma1.it

In this Letter, the first implementation, to our knowledge, of X-junctions between photorefractive soliton waveguides in lithium niobate-on-insulator (LNOI) films is reported. The experiments were performed on 8 μm thick films of congruent undoped LiNbO₃. Compared with bulk crystals, the use of films reduces the soliton formation time, allows more control over the interaction between the injected soliton beams, and opens a route to integration with silicon optoelectronics functions. The created X-junction structures show effective supervised learning, directing the signals propagated inside the soliton waveguides into the output channels highlighted by the control assigned by the external supervisor. Thus, the obtained X-junctions have behaviors analogous to biological neurons.   © 2022 Optica Publishing Group

Spatial solitons have been extensively investigated in the past decades [1–10]. Among all the possible nonlinearities capable of inducing soliton confinement, photorefractivity [6–10] shows the greatest versatility and ease of implementation. Being a saturating nonlinearity, it allows stable two-dimensional confinement but, above all, it can form at very low optical powers (nanowatts to microwatts). Moreover, the modification of the refractive index induced by the soliton beam acts as a real waveguide [5,10]. These features make photorefractive media unique for exploiting such "plasticity" of the refractive index. Not only can single interconnections or entire circuits be written with very low powers [11,12], but these integrated structures are also fully addressable, in the sense that they can be written, modified, or erased in order to perform transient interconnections and signal processing. Recently, soliton waveguides were utilized in bulk LiNbO₃ in the form of X-junctions, able to address signal information toward different outputs, performing tasks typical of machine learning [13–15]. Precisely, soliton X-junctions can behave like photonic neurons, realizing both supervised and unsupervised information memorization and recognition [15]. A recent study [16] has shown that, by connecting a number of neural solitonic units, it is possible to create complex networks that are able to resolve advanced problems, such as image recognition, information storage, and reproduction of episodic psycho-memory.

Conversely, being linked to the photogeneration and displacement of electric charges, photorefractivity (PR) is usually slow:

the fastest response can be observed in III–V semiconductors, such as InP [17,18], for which solitons are formed in tens of milliseconds. Among the dielectric bulk crystals, a fast response was observed, for example, in BSO [19] or SBN [20], while some media, such as LiNbO₃ [10], have proved to be rather slow. This is a real shame, because LiNbO₃ is available at high quality and possesses useful properties, such as large electro-optical and nonlinear coefficients, which make it the most used material in active integrated optical devices. Recently, Chauvet *et al.* [21] demonstrated that the soliton formation time in LiNbO₃ crystals can be drastically reduced by two orders of magnitude by using films instead of bulk crystals. There are other advantages in the use of LiNbO₃ films (LNFs); not only is there the PR process speed-up, but LiNbO₃-on-insulator (LNOI) films may interface with integrated silicon photonic circuits, giving them the nonlinear active response that silicon lacks in the optical domain. Moreover, LNOI devices can be directly coupled with electronic circuits [22,23], providing an enormous processing capacity, thanks to hybrid optoelectronic platforms. In this Letter, we demonstrate that addressable solitonic X-junctions can be efficiently generated in LNFs. LNF samples were fabricated from photonic grade *z*-cut 500 μm thick undoped LiNbO₃ wafers. A buffer layer of silica (typically 1 μm) is first deposited on one face of the wafer, followed by the sputtering of a gold layer, typically 200 nm. A similar gold layer is then deposited on a high-flatness silicon wafer. Both wafers are then placed in contact and pressed to form a strong gold bond. Finally, the formed heterostructure is ground and polished to give a slab waveguide consisting of an 8 μm thick LiNbO₃ layer on a silicon substrate with silica and gold buffer layers. This hybrid wafer is finally cut using a precision saw to form rectangular samples with polished faces. The complete procedure of fabrication of the samples, as well as their exact geometry, can be found in the paper by Chauvet *et al.* of 2015 [21].

The experimental setup is shown in Fig. 1(a). A 532-nm CW laser beam is divided into two collimated beams using a Mach–Zehnder delay line, set longer than the coherence length, to have two incoherent beams. Their mutual power ratio is controlled using neutral density filters. The Mach–Zehnder output recombining beam splitter sets a small angular deviation between the two beams, as shown in Fig. 1(b). This angular deviation is magnified by a focusing lens placed at focal distance from the entrance face of the sample. This apparatus generates two focused light beams of about 10 μm FWHM at the entrance
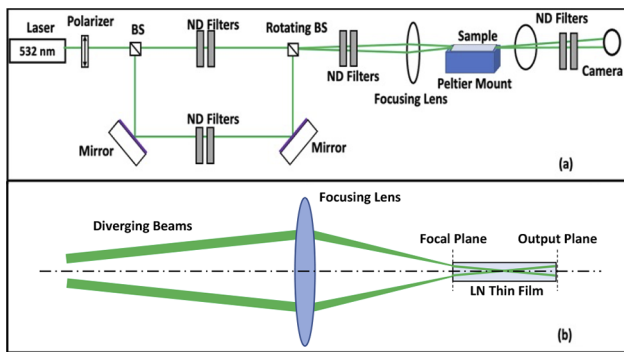
Fig. 1. (a) Experimental setup for formation of X-junctions. (b) Detailed top view of trajectories of two beams before and inside slab LiNbO$_3$ waveguide.

face of the LNF (as long as five diffraction lengths), crossing at the center of it at an angle of approximately 1°. Careful alignment allows light coupling to the fundamental mode of the slab waveguide, giving two extraordinarily polarized guided waves. The output face of the waveguide is imaged onto a camera using a magnifying optical system. The photorefractive effect is controlled by the pyroelectric effect [21,24], which generates an internal electric field oriented perpendicularly to the LiNbO$_3$ layer that is along the crystal c-axis. The amplitude of this field is proportional to the temperature change ΔT compared with the initial sample temperature. For this purpose, the sample is placed on a holder whose temperature is raised by a Peltier element up to +15°C.

During the few seconds of heating thermalization, the two beams are blocked to avoid any uncontrolled photorefractive modification.

Initially, two crossing beams of the same power (10 μW) are used to write the X-junction. In Fig. 2(a), the linear diffraction of these beams is shown. Letting the temperature vary, the photorefractive nonlinearity acts and the two beams self-confine [Fig. 2(b)] down to the same input waists; the process is considered completed when a stable stationary regime is reached, giving rise to solitonic beams.

Now that the junction is formed, a low-power signal (10 nW) is injected inside one of the two input channels. The balanced symmetrical junction splits this signal 50–50 (48.9–51.1) toward both output channels, as shown in Fig. 2(c). Varying the relative powers of the writing crossing beams, asymmetrical X-junctions can be generated too. For example, fixing the power of one channel to be twice that of the other one (20 μW versus 10 μW), the resulting X-junction is unbalanced toward the highlighted output one. Consequently, the probe signal is switched asymmetrically 70–30 (70.3–29.7) toward the highlighted channel, as depicted in Fig. 2(d), where the right channel is the stronger.

For a power ratio of three between the two writing beams, the probe signal is divided asymmetrically 80–20 (80.4–19.6), as depicted in Fig. 2(e). By choosing a specific power ratio during the writing process, we have the possibility of adjusting the splitting rate (Fig. 3). Similar features were observed in bulk lithium niobate too [13–16], demonstrating that the maximum splitting ratio that can provide a photoinduced X-junction is about 80–20.

Additionally, an important feature to be stressed is that the described splitting behavior of the junction does not depend on
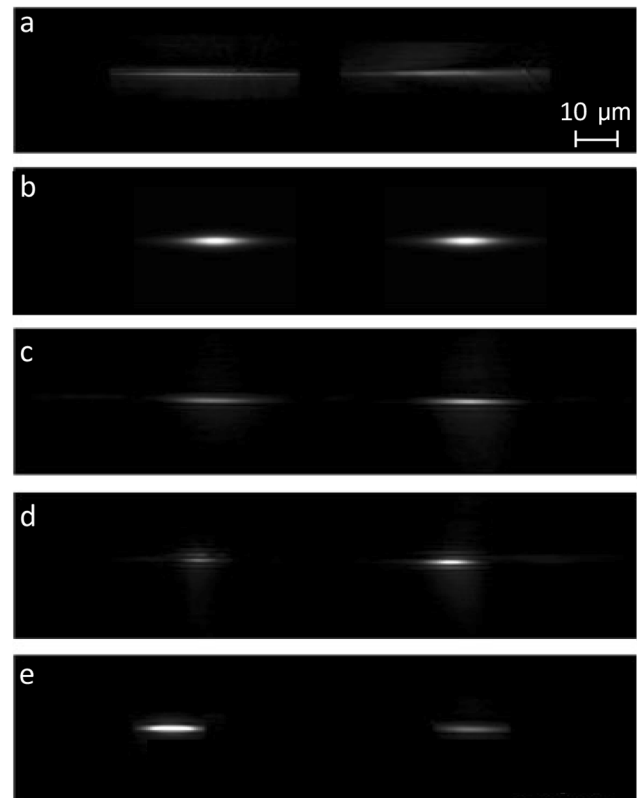

Fig. 2. Light distributions on output face of waveguide of LiNbO3 plate: (a) diffraction of beam in linear regime; (b) soliton regime of two beams of the same intensity; (c) a low-power signal divides 50–50 in a balanced soliton junction; (d) if one channel of the junction is written by a double power with respect to the other, the signal will divide 70–30 toward this highlighted output; (e) if one channel of the splice is written by a triple power of the other, the signal will divide 80–20 toward this highlighted output.
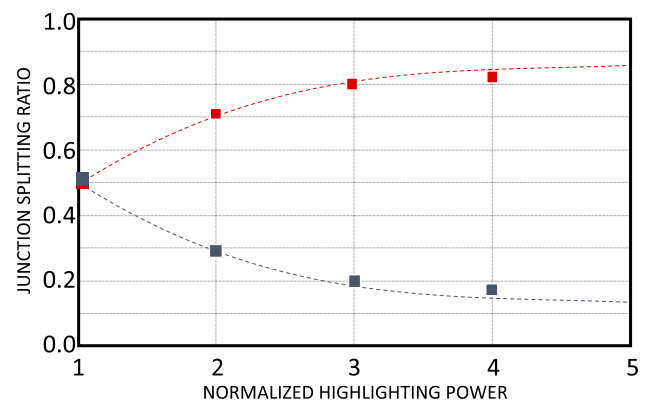

Fig. 3. Experimental splitting ratios plotted together with theoretical trends as a function of the highlighting power normalized to the other channel power.

the input channel in which the probing signal is injected, but only on the power ratio between the writing beams.

This assertion is illustrated in Fig. 4 for a 70–30 splitting X-junction. If the probe signal is injected in the highlighting channel [Fig. 4(a)] or in the nonhighlighting one [Fig. 4(b)], the higher output (70%) will always come out from the highlighting
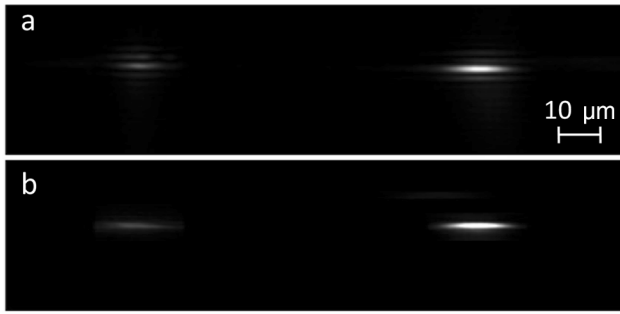
Fig. 4. Light distribution at output face of LiNbO$_3$ slab waveguide in the case of an imbalance 70–30 X-junction, for probe signal injected in: (a) highlighting input channel; (b) nonhighlighting input channel.
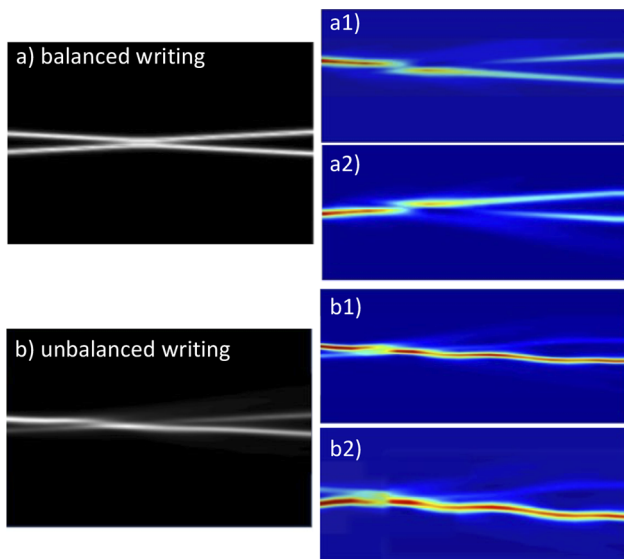

Fig. 5. Numerical simulation of X-junction behavior. (a) Writing process of a balanced junction and (a1), (a2) its signal splitting behaviors depending on the probed input. (b) Similar simulations for the writing of an unbalanced junction and (b1), (b2) its signal behaviors.

channel, it being the more contrasting channel, while the smaller power (30%) will come out from the other one. This feature is a consequence of the interaction zone between the soliton channels, which homogenizes the input signals regardless of where they come from and directs them exclusively based on the refractive index contrast of the junction-output channels.

In this way, the junction learns the information sent by the supervisor, which defines which of the two channels is the one highlighted (supervised learning).

To illustrate and have some insight to the coupled waveguides, computer simulations are presented in Fig. 5, using a well-tested finite-difference time-domain (FDTD) numerical code [15,16]. Such code solves the nonlinear wave equation where a saturating nonlinear dielectric constant is considered. In the figure, the light distributions at the end of the writing process of balanced [Fig. 5(a)] and unbalanced [Fig. 5(b)] junctions are depicted. The corresponding signal splitting evolutions in the so-formed balanced X-junctions are shown when probed from one input
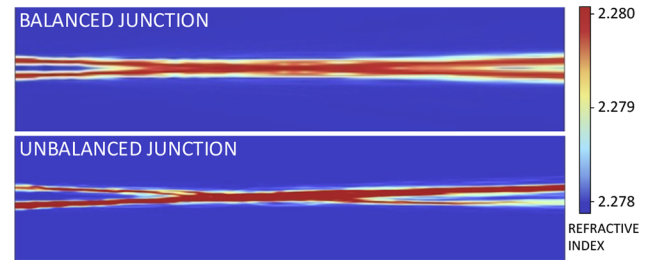

Fig. 6. Numerical maps of X-junction refractive index for balanced and unbalanced regimes.

[Fig. 5(a1)] or from the other one [Fig. 5(a2)]. A balanced junction divides the signal into equal parts [Figs. 5(a1) and 5(a2)]. An unbalanced junction sends full power to the highlighting output, independently of the excited input [Figs. 5(b1) and (b2)].

This process generates an asymmetrical distribution of the refractive index that drives the signal to exit from the highlighting channel (Fig. 6).

The development of a specific model for LNFs is beyond the range of this paper but it is important to emphasize that, even though pyroelectric spatial solitons in bulk LiNbO$_3$ and films of LiNbO$_3$ both rely on the photorefractive effect, the underlying physics is, however, very different. Indeed, that light-induced self-focusing in bulk occurs is due to the well-known classical combined effects of charge photogeneration and transport owing to drift by the pyroelectric electric field, followed by charge recombination on deep centers in the dark area that leads to the nonuniform screening of the electric field, finally inducing the refractive index distribution responsible for the self-guiding. In the LNF, a simpler mechanism is foreseen. The main reason is that the light guided in the slab waveguide constituted of LiNbO$_3$ fills the entire thickness of the film. Consequently, this light bridges the gap between free charges of opposite signs that are present on the Z$^+$ and Z$^-$ faces of the medium, to compensate the spontaneous polarization of LiNbO$_3$. The increased conductivity induced by light allows a current to flow between opposite z-faces, giving rapid electron–hole recombination. This leads to the decay of the pyroelectric field in the illuminated region and to the nonuniform refractive index distribution at the origin of self-guiding. Self-focusing in z-cut LNFs is thus a consequence of the neutralization of a charged area, rather than the formation of a PR space charge field. This is at the origin of the very different observed dynamics in film and in bulk LiNbO$_3$. However, despite these major differences, we have shown that LNF is a convenient medium to induce X-junctions. More complex functions can be envisioned.

In conclusion, we have experimentally shown the possibility of creating all-optical addressable X-junctions in slab waveguides made of LiNbO$_3$ on silicon (LNOI) using a photorefractive self-focusing mechanism controlled by a pyroelectric effect.

Such waveguide junctions are able to split incoming light depending on writing beams that can be considered as supervisors (supervised learning). This has been demonstrated to be an efficient way to reproduce characteristic neural behaviors, such as plasticity and adaptability. Therefore, the LiNbO$_3$ layer's ability to form X-junctions suggests that it may act as a neural photonic unit characterized by important advantages deriving from LNF technology. Among its advantages are the provision of a better control of the mutual coupling of the input beams, along with their propagation, a crystal response two orders of

magnitude faster than in bulk, and the possibility of being easily integrated in more complex devices. This configuration also brings a great potential to control the propagation of self-trapped waves by external beams incoming from the top surface.

Disclosures. The authors declare no conflicts of interest.

Data availability. Data underlying the results presented in this paper are not publicly available at this time but may be obtained from the authors upon reasonable request.

REFERENCES

1. V. I. Bespalov and V. I. Talanov, Sov. Phy. JETP Lett. **3**, 307 (1966).
2. A. Barthelemy, S. Maneuf, and C. Froehly, Opt. Commun. **55**, 201 (1985).
3. S. Maneuf, R. Desailly, and C. Froehly, Opt. Commun. **65**, 193 (1988).
4. J. S. Aitchison, A. M. Weiner, Y. Silberberg, M. K. Oliver, J. L. Jackel, D. E. Leaird, E. M. Vogel, and P. W. E. Smith, Opt. Lett. **15**, 471 (1990).
5. R. de la Fuente, A. Barthelemy, and C. Froehly, Opt. Lett. **16**, 793 (1991).
6. Y. Chen, Opt. Lett **16**, 4 (1991).
7. M. Segev, B. Crosignani, A. Yariv, and B. Fischer, Phys. Rev. Lett. **68**, 923 (1992).
8. M. Segev, G. C. Valley, B. Crosignani, P. DiPorto, and A. Yariv, Phys. Rev. Lett. **73**, 3211 (1994).
9. V. Tikhonenko, J. Christou, and B. Luther-Davies, Phys. Rev. Lett. **76**, 2698 (1996).
10. E. Fazio, F. Renzi, R. Rinaldi, M. Bertolotti, M. Chauvet, W. Ramadan, A. Petris, and V. I. Vlad, Appl. Phys. Lett. **85**, 2193 (2004).
11. Z. Xu, Y. V. Kartashov, and L. Torner, Opt. Express **13**, 1774 (2005).
12. Z. Xu, Y. V. Kartashov, L. Torner, and V. A. Vysloukh, Opt. Lett. **30**, 1180 (2005).
13. M. Alonzo, D. Moscatelli, L. Bastiani, A. Belardini, C. Soci, and E. Fazio, Sci. Rep. **8**, 5716 (2018).
14. B. Ianero, A. Bile, M. Alonzo, and E. Fazio, J. Comput. Electron. **20**, 2614 (2021).
15. A. Bile, F. Moratti, H. Tari, and E. Fazio, Neural. Comput. Applic. **33**, 17071 (2021).
16. A. Bile, H. Tari, and E. Fazio, Appl. Sci. **12**, 5585 (2022).
17. D. Wolfersberger, N. Khelfaoui, C. Dan, N. Fressengeas, and H. Leblond, Appl. Phys. Lett. **92**, 021106 (2008).
18. M. Alonzo, C. Dan, D. Wolfersberger, and E. Fazio, Appl. Phys. Lett. **96**, 121111 (2010).
19. E. Fazio, W. Ramadan, A. Belardini, A. Bosco, M. Bertolotti, A. Petris, and V. I. Vlad, Phys. Rev. E **67**, 026611 (2003).
20. M. Shih, P. Leach, M. Segev, M. H. Garrett, G. Salamo, and G. C. Valley, Opt. Lett. **21**, 324 (1996).
21. M. Chauvet, F. Bassignot, F. Henrot, F. Devaux, L. Gauthier-Manuel, H. Maillotte, G. Ulliac, and B. Sylvain, Opt. Lett. **40**, 1258 (2015).
22. M. Rusing, P. O. Weigel, J. Zhao, and S. Mookherjea, IEEE Nanotechnology Mag. **13**, 18 (2019).
23. M. G. Vazimali and S. Fathpour, Adv. Photonics **4**, 034001 (2022).
24. J. Safioui, F. Devaux, and M. Chauvet, Opt. Express **17**, 22209 (2009).